The jet and the disk of the HH 212 low-mass protostar imaged by ALMA: SO and SO2 emission

L. Podio, C. Codella, F. Gueth, S. Cabrit, R. Bachiller, A. Gusdorf, C.-F. Lee, B. Lefloch, S. Leurini, B. Nisini, and M. Tafalla

- ALMA (Cycle 0), 345 GHz band
- SO, SO_2 , $C^{17}O$, CO, SiO)
- Kinematics for jet and outflow from a Class 0 protostar
- SO and SO_2 compared to CO, SiO…

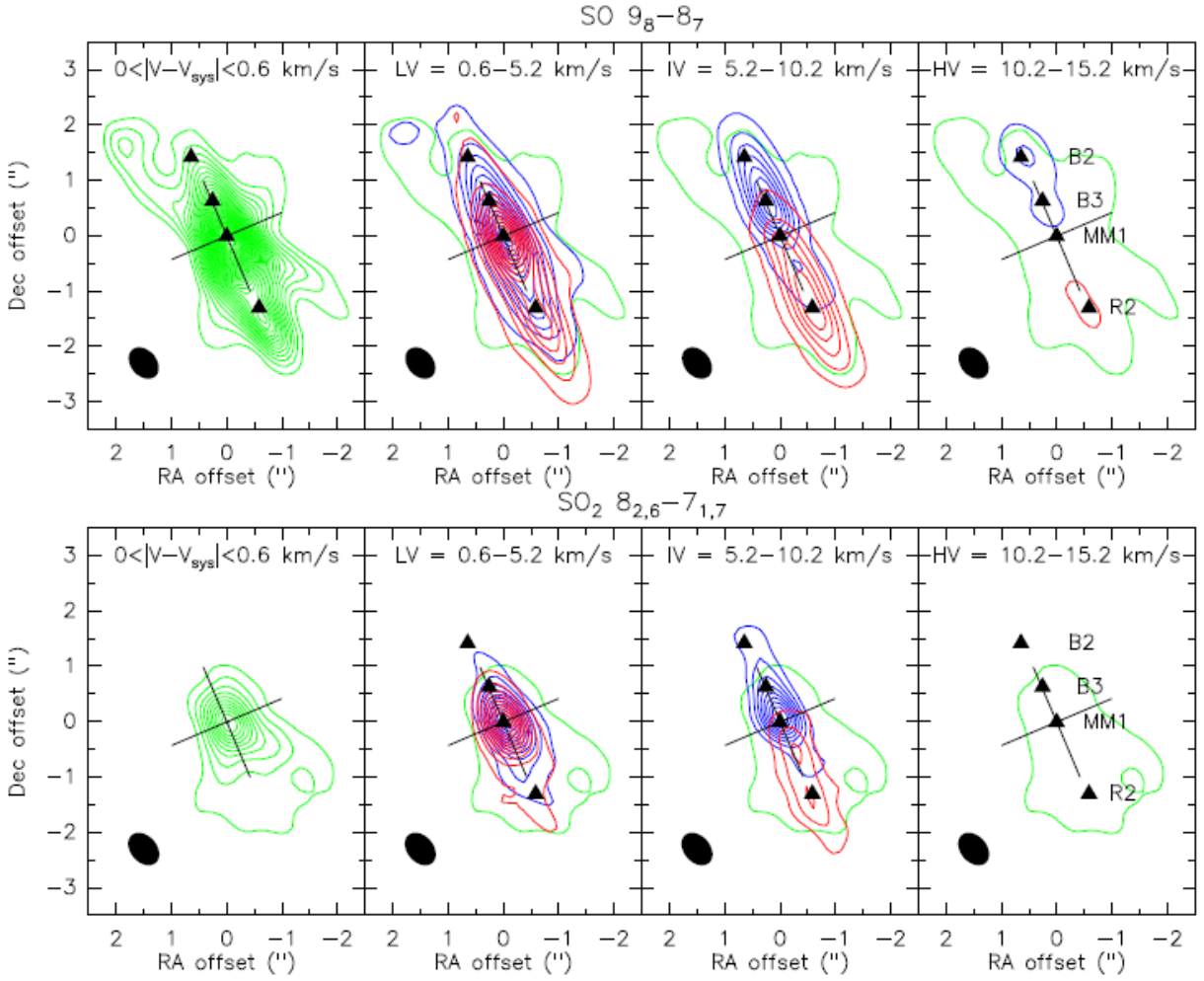

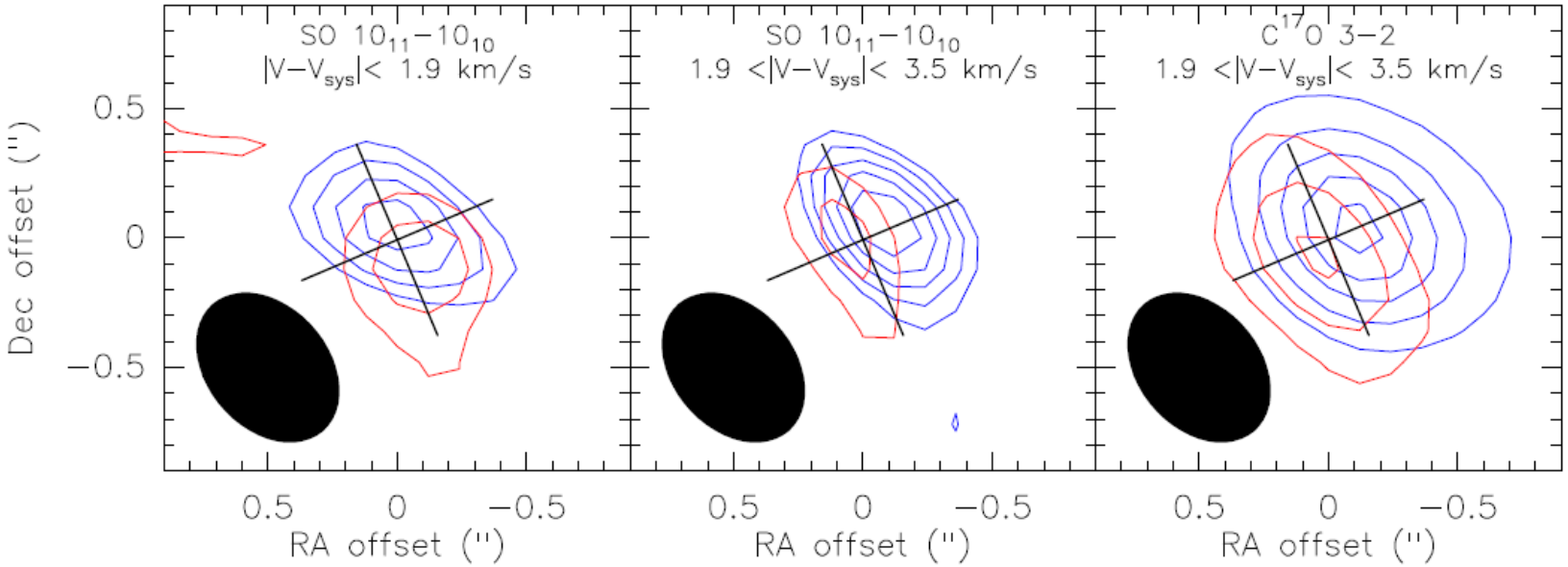

- SO and SO2 are effective tracers of the molecular jet in the inner few hundreds AU from the protostar.
- The SO abundance in the disk is 3 – 4 orders of magnitude larger than in evolved protoplanetary disks. This may be due to an SO enhancement in the accretion shock at the envelope-disk interface or in spiral shocks if the disk is partly gravitationally unstable.

A universal, turbulence-regulated star formation law: from Milky Way clouds to highredshift disk and starburst galaxies

Diane M. Salim, Christoph Federrath and Lisa J. Kewley

- previous study: In K-S law, the observed scatter in Σ_{SFR} (for a given Σ_{gas} or Σ_{gas}/t_{ff}) can be primarily attributed to the variation in the sonic Mach number of the turbulence in the star-forming clouds.
- Problem in previous work by Krumholz et al. (2012)
  - Refinement was achieved by expressing the K-S law with Σ_{gas}/t_{ff}
  - The model uses averaged surface density and average freefall time. The wide distribution of densities withint the ISM/clouds is not taken into account.

  → incorporate the probability density function (PDF) in this study, and multi-freefall concept (t_{ff} depends on the density)

$$\int [\Sigma_{\rm gas}(\rho)/t_{\rm ff}(\rho)]\, p_\rho d\rho = \Sigma_{\rm gas}(\rho_0)/t_{\rm ff}(\rho_0) \quad \text{X} \quad \exp(3\sigma_s^2/8),$$

$$p(s)ds = \frac{1}{\sqrt{2\pi\sigma_s^2}} \exp\left(-\frac{(s-s_0)^2}{2\sigma_s^2}\right) ds, \quad s = \ln(\rho/\rho_0). \qquad \sigma_s^2 = \ln\left(1 + b^2\mathcal{M}^2 \frac{\beta}{\beta+1}\right),$$

New SF law

$$\Sigma_{\rm SFR} = 0.4\% \times \left(\Sigma_{\rm gas}/t\right)_{\text{single-ff}} \times \left(1 + b^2\mathcal{M}^2 \frac{\beta}{\beta+1}\right)^{3/8}$$

- Observations: 11 galactic, SMC
- Better fit by a factor of 3—4 (goodness-of-fit $R^2 = 0.97$)

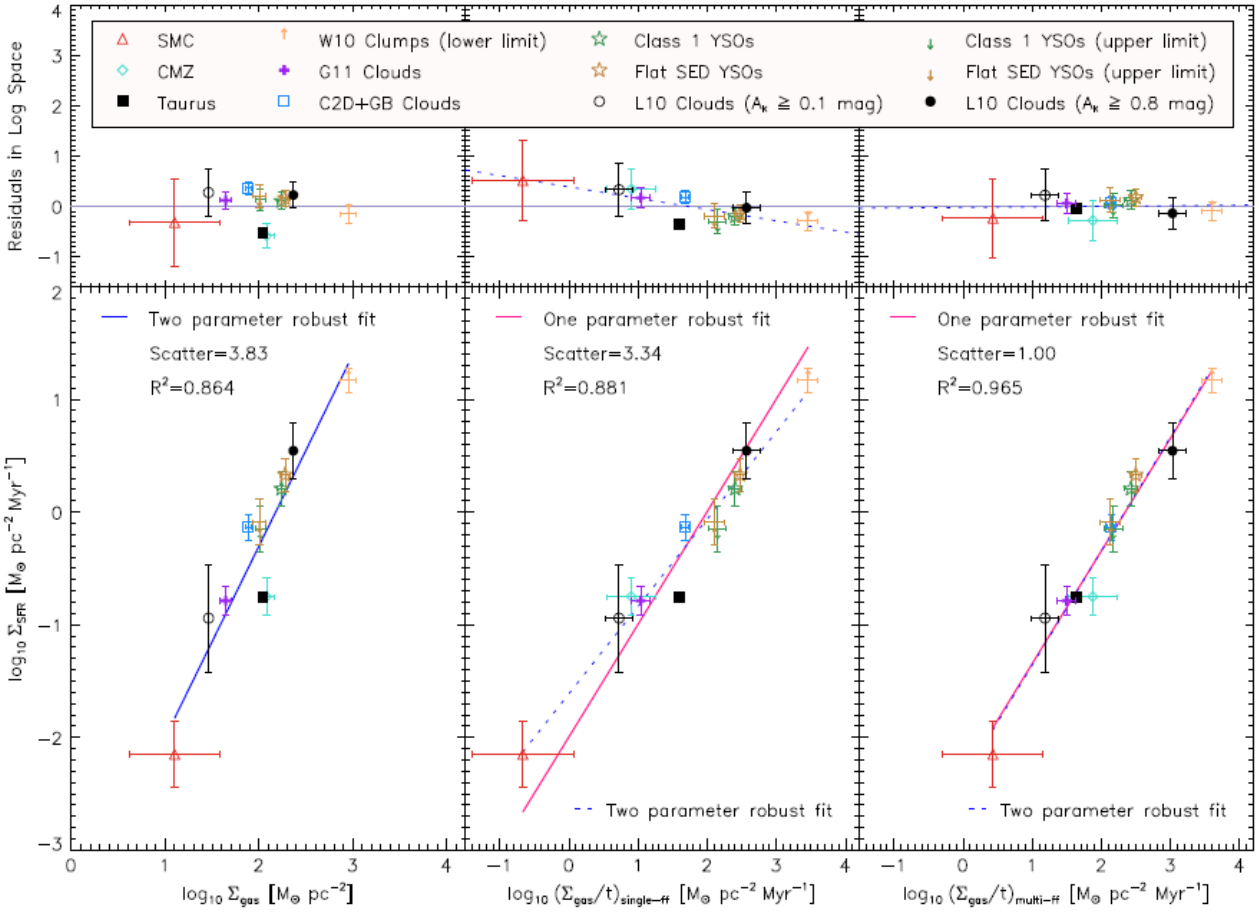

Figure 2. Bottom panels: Σ_{SFR} vs. Σ_{gas} (classical Kennicutt–Schmidt relation; left), Σ_{SFR} vs. $(\Sigma_{gas}/t)_{single\text{-}ff}$ (Krumholz et al. 2012; middle), and our new model, Σ_{SFR} vs. $(\Sigma_{gas}/t)_{multi\text{-}ff}$ (right) for the observational data in Table 1. Power-law fits are shown as solid lines and the respective goodness-of-fit parameter R^2 (where $R^2 = 1$ corresponds to a perfect fit) is shown in each panel, as well as the normalized scatter. We also apply a two-parameter robust line fit to these relations, shown as the dotted lines. We find that our new multi-freefall SF law provides the best correlation with a reduced scatter by a factor of 3–4 compared to the previous SF laws. Top panels: the residuals of each relation in log space vs. each of the parameterizations being analyzed. The solid and dotted lines in each panel are respectively the fits shown in the bottom panels.

Mach number can be predicted for extragalactic sources using the new SF law.

Table 3
ictions for Extragalactic Systems Obtained by
Our Improved SF Law, Equation (10)

Redshift	Galaxy Type	$\mathcal{M}$ Estimate
~0	Disk	$4.0^{+2.0}_{-1.7}$
~0	Starburst	$13^{+21}_{-9.4}$
1–3	Disk	16^{+25}_{-11}
1–3	Disk	18^{+21}_{-10}
Genzel et al. (2010)	1–3	Disk	$5.7^{+0.5}_{-0.4}$
	1–3	Starburst	51^{+120}_{-36}
Bouché et al. (2007)	1–3	Starburst	71^{+120}_{-45}

V409 Tau As Another AA Tau: Photometric Observations of Stellar Occultations by the Circumstellar Disk

Joseph E. Rodriguez, Joshua Pepper, Keivan G. Stassun, Robert J. Siverd, Phillip Cargile, David A. Weintraub, Thomas G. Beatty, B. Scott Gaudi, Eric E. Mamajek, Nicole Sanchez

- Optical photometric monitoring of AA Tau and V409 Tau
- good use of data/instruments for exoplanetary transits
- AA Tau & V409 Tau
  - Showing short-timescale variation (day—week)
- AA Tau
  - Deep, dimming event in 2011, lasting at least until winter in 2013
  - Occultation by dense part of the disk at >8 AU ($M_* = 0.85\ M_\odot$).

  [Confirmation of Bouvier et al. (2013)]
  - i~71 deg, a=7.7 AU → h=7.7 AU for the occulter

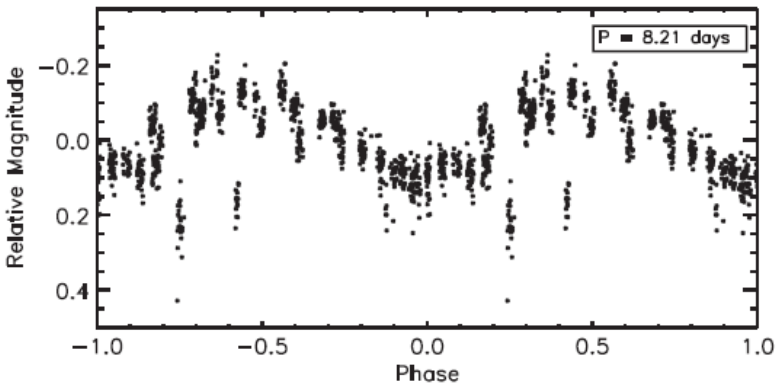

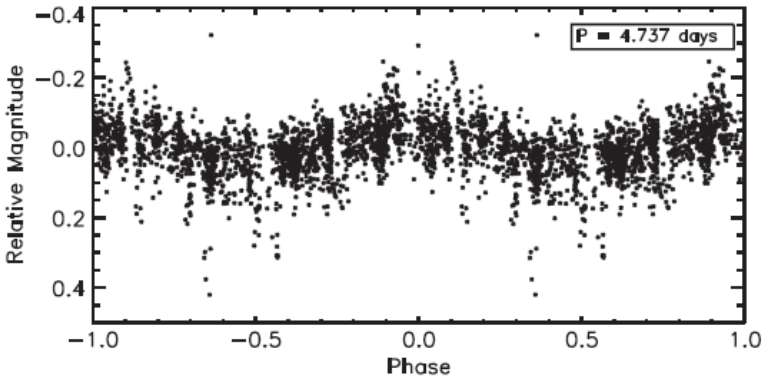

- V409 Tau
  - AA Tau-type variable
  - SED → i~81 deg, $M_* = 0.57\ M_\odot$
  - 2 events of deep dimming

    (1) from 2009 Jan—late 2010 Oct

    (2) from 2012 Mar to at least 2013 Sep.

    [another event in 1960's]
  - Duration >600 days, depth ~1.4 mag
  - Duration → width of a warp =2.5 AU
  - Assumed period ~46.25 years (1962—2009)

  → High-density feature at >~10 AU, h=2 AU
  - Assumed period ~1130 days (between 2009 and 2012 events

  →High-density feature at ~2 AU, h=0.3 AU

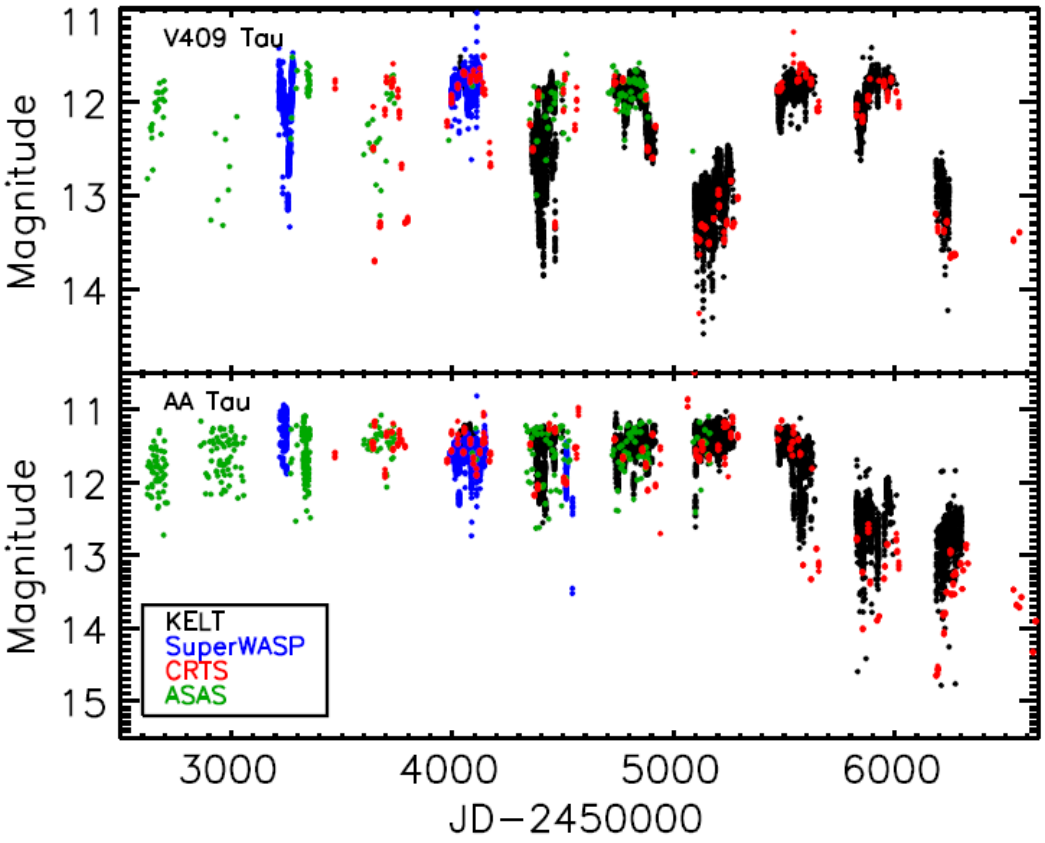

From 2004 to 2013, (roughly) in V,R band

Hot dust revealed during the dimming of the T Tauri star RW Aur A

Victor Shenavrin, Peter Petrov and Konstantin Grankin

- IR photometric monitoring of RW Aur AB system
- RW Aur AB
  - ρ = 1.4”, 1.4 $M_\odot$ + 0.8 $M_\odot$
- RW Aur B
  - WTTS (weak accretion)
  - ρ =0.12”, M_3<0.045 $M_\odot$
- Variability in previous study
  - Long-lasting dimming event in 2010

    Duration of several month, depth~2 mag in optical

    Obscuration by tidally-disrupted disk?
  - Dimming event in 2014, faded by ~3 mag

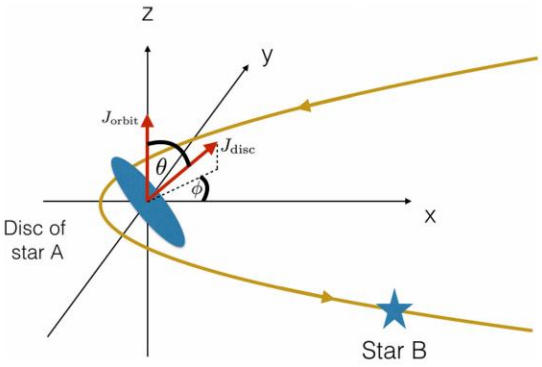

Dai et al. (2015)

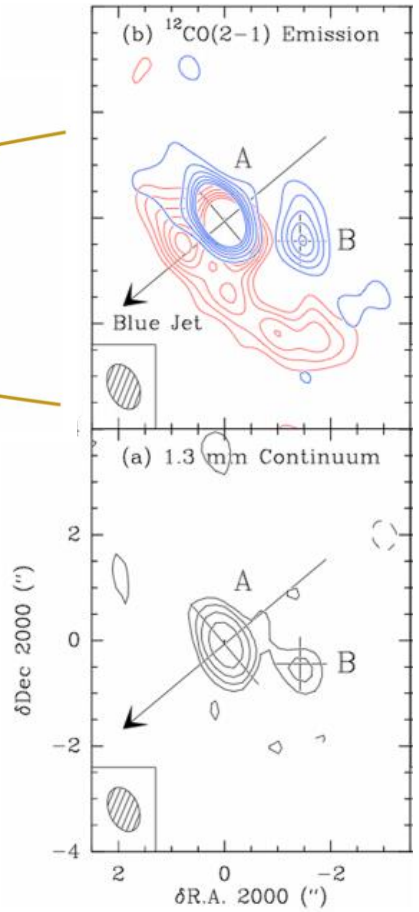

Cabrit et al. (2006)

- IR photometry (1—5 micron) with 125cm telescope (A and B are not resolved. Most IR emission comes from A.)
- IR slope is different between the brighter and fainter phases. When the star fades in optical, additional ~1000 K body is required

  → hot dust near the dust sublimation temp (~0.1-0.2 AU)? UXOri-like variability? (should not be the occultation by the distant arm)
- Disk inclination=30—45 deg. Accretion rate remained as usual.

  → Dust in the wind? (the wind was enhanced during the event)

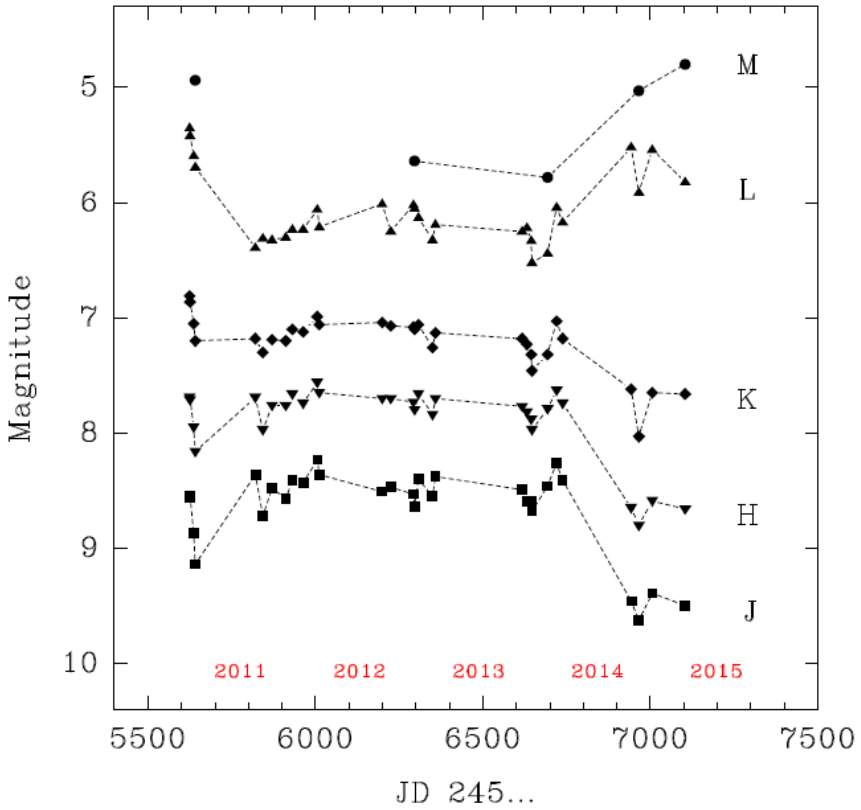

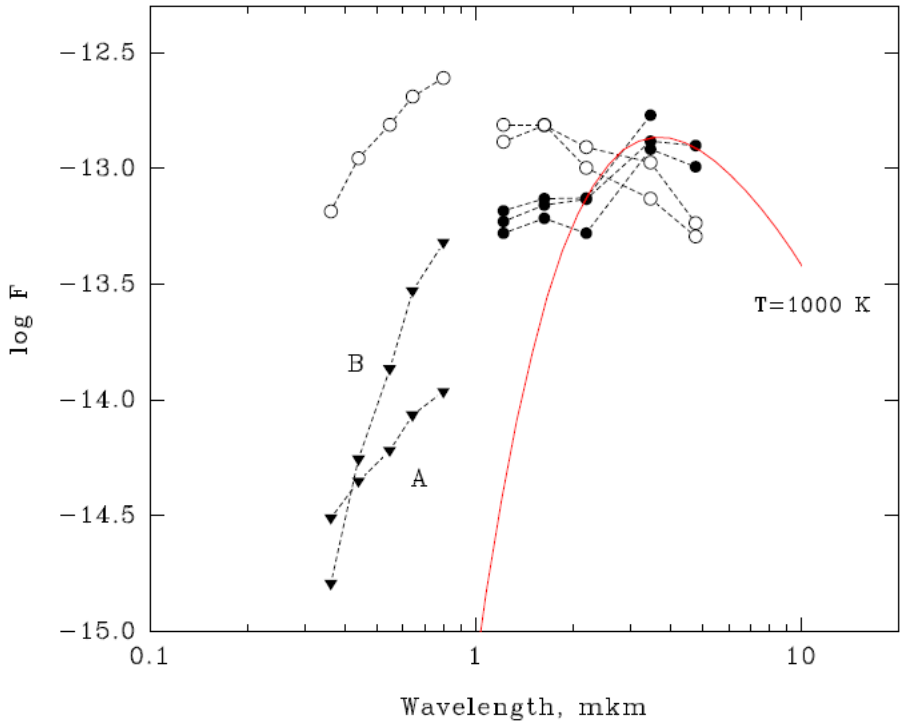

Dense Clumps and Candidates for Molecular Outflows in W40

Tomomi Shimoikura, Kazuhito Dobashi, Fumitaka Nakamura, Chihomi Hara, Tomohiro Tanaka, Yoshito Shimajiri, Kouji Sugitani and Ryouhei Kawabe

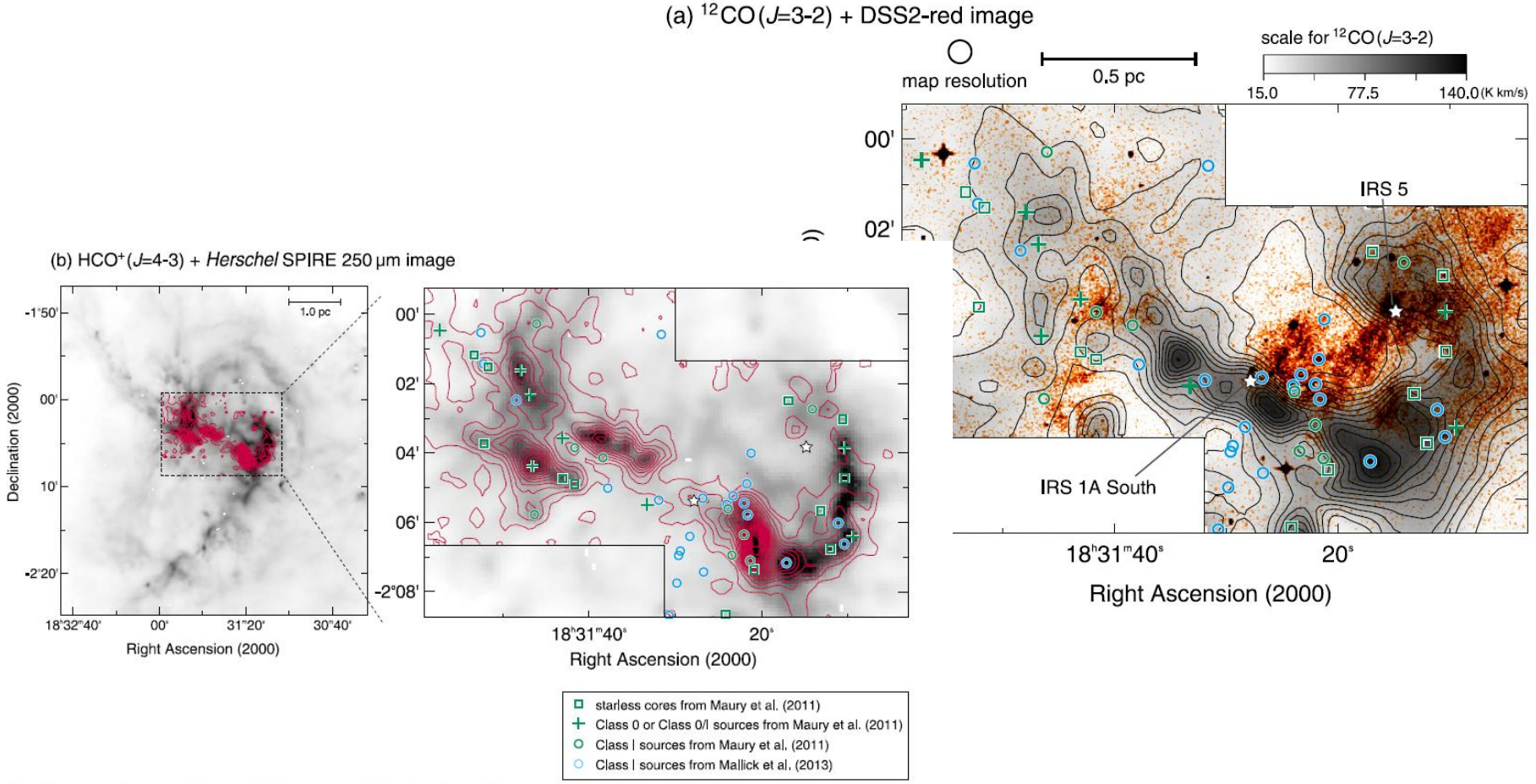

Figure 1. Integrated intensity maps of the (a) ^{12}CO ($J = 3–2$) emission line and (b) HCO$^+$ ($J = 4–3$) emission line around W40 obtained with the ASTE telescope. Velocity ranges used for the integration are $-3.0 \leqq V_{LSR} \leqq 15.0$ km s^{-1} and $3.0 \leqq V_{LSR} \leqq 11.4$ km s^{-1} for the ^{12}CO and HCO$^+$ maps, respectively. The lowest contours and the contour intervals for the map in panel (a) are 10 K km s^{-1}, and those in panel (b) are 1 K km s^{-1}. The red color scale in panel (a) is the DSS2-red image, and the gray scale in panel (b) is the *Herschel* SPIRE 250 μm image. Positions of the high-mass IRS sources (IRS 1 A South and IRS 5, Shuping et al. 2012) are indicated by star marks. Squares, plus signs, and circles denote the starless cores and Class 0/I sources classified by Maury et al. (2011) (colored in green) and Mallick et al. (2013) (colored in blue). The map resolution (31″) and a linear scale of 0.5 pc (at $D = 500$ pc) are shown at the top of panel (a). The area enclosed by the thin lines in panel (a) and right side of panel (b) denotes the observed region.

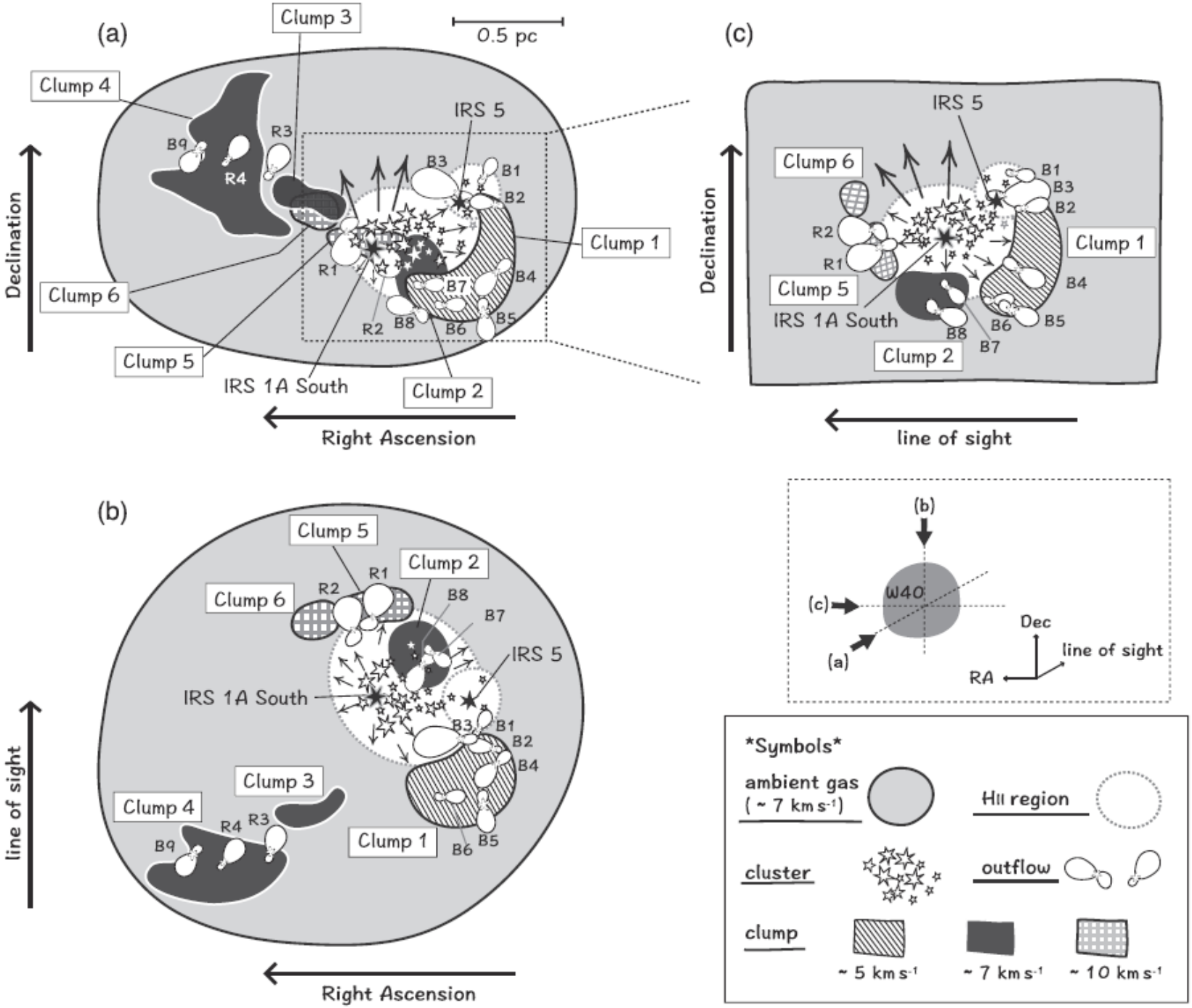
(a)
Clump 3
0.5 pc
Clump 4
IRS 5
R3
B9
R4
B3
B1
B2
Clump 1
Declination
R1
B4
Clump 6
B7
R2
B8
B6
B5
Clump 5
IRS 1A South
Clump 2
Right Ascension
(c)
IRS 5
Clump 6
B1
B3
B2
R2
Clump 1
R1
B4
Clump 5
IRS 1A South
B8
B6
B5
B7
Clump 2
Declination
line of sight
(b)
Clump 5
Clump 2
R1
Clump 6
R2
B8
B7
IRS 5
IRS 1A South
B3
B1
B2
B4
Clump 3
Clump 4
R4
R3
B9
Clump 1
B6
B5
line of sight
Right Ascension
(b)
(c)
W40
(a)
Dec
line of sight
RA
Symbols
ambient gas
(~ 7 km s-1)
HII region
cluster
outflow
clump
~ 5 km s-1
~ 7 km s-1
~ 10 km s-1